Preliminary Design of Low-Energy Low-Thrust Transfers to Halo Orbits using Feedback Control

Bindu B Jagannatha*, Jean-Baptiste H. Bouvier† and Koki Ho‡
University of Illinois at Urbana-Champaign, Urbana, IL, 61801

Calculating low-thrust trajectories that connect geocentric orbits to Earth-moon halo orbits involves designing the many-revolution thrust arc required to depart Earth vicinity. Existing methods are based on solving the corresponding optimal control problem and hence are computationally expensive, involve providing hard-to-obtain initial guesses, and do not lend themselves well to quick parametric trade studies. In this paper, a stochastic optimization algorithm is coupled with a Lyapunov feedback control law to explore the solution space for designing Earth-to-halo low-energy low-thrust trajectories. While the objective is to minimize the fuel consumed for the transfer, the time of flight is constrained so as to optimally distribute the coast time between the low-thrust escape spiral and the low-energy arc. Engines are assumed to have a constant specific impulse and provide constant thrust throughout the transfer. The results obtained from this method are then compared with other available reference solutions in order to quantify its effectiveness in designing such transfers. Favorable comparisons thus obtained demonstrate the utility of the proposed method in calculating almost-optimal solutions, combined with a large improvement in computation time.

I. Introduction

Dynamical structures inherent to the circular restricted three-body system have been shown to play a significant role in the design of optimal spacecraft trajectories [1, 2]. These structures provide low-energy pathways in the cislunar region that are of specific interest for potential applications in space infrastructure deployment. Within this region, the unstable halo orbits around the collinear Earth-moon Lagrange points L_1 and L_2 are being examined to serve as staging nodes for expansion of human space activities [3]. Trajectories that leverage these unstable periodic orbits and their associated invariant manifolds allow transfers within the cislunar region for lower costs than the conventional ones [4].

Achieving these same transfers with low-thrust propulsion is currently a growing research field because higher mass fractions can be delivered, albeit at the cost of longer times of flight. A sample low-thrust trajectory between Earth and

*PhD Candidate, Aerospace Engineering, 306 Talbot Laboratory, MC-236, 104 South Wright Street, Urbana, Illinois 61801
†Master's Student, Aerospace Engineering, 306 Talbot Laboratory, MC-236, 104 South Wright Street, Urbana, Illinois 61801
‡Assistant Professor, Aerospace Engineering, 306 Talbot Laboratory, MC-236, 104 South Wright Street, Urbana, Illinois 61801

a halo orbit can be conducted by breaking up the journey into two phases – a spiral thrust arc that departs the given Earth parking orbit and targets the invariant manifolds associated with the halo orbit, followed by a coast arc on the manifold. Previous studies have used different thrusting strategies to design such transfers by casting them into optimal control problems and using gradient-based techniques like nonlinear programming (NLP) to solve them. Senent et al. [5] studied low-thrust transfers to libration point orbits in the sun-Earth/moon system via their manifolds using *variable* specific impulse engines. A similar problem in the Earth-moon three-body system was solved by Ozimek and Howell [6] by employing iterative continuation to lower the thrust value until problem constraints were satisfied. Other efforts by Mingotti et al. [7–11] used the concept of attainable sets to seed initial guesses for low-thrust low-energy transfers in the Earth-moon system and sun-perturbed Earth-moon system, as well as in the sun-Earth/moon system. Constant specific impulse engines were assumed for these trajectories. Martin and Conway [12] further refined the solution to the Earth-to-halo transfer problem by including the low-thrust escape spiral as a part of the optimization setup. Optimal low-thrust low-energy transfers commencing with ballistic escape from Earth-orbit (i.e., impulsive maneuver provided by launch vehicle) in patched three-body problems have also been studied [13, 14].

Solving these optimal control problems usually requires the mission designer to seed initial guesses using an understanding of the underlying dynamics (e.g., through the use of Poincaré sections) or generate them by solving a homotopically similar problem or continuation techniques. This task can be non-trivial and time consuming. Additionally, solving the fully-formulated optimal problem can be computationally intensive as it can suffer from the curse of dimensionality typically associated with transfers consisting of significant spiraling (on the order of tens or hundreds of revolutions) and the iterative nature of NLP methods. Since these methods usually consume substantial computational resources to generate single point solutions, they also do not lend themselves well to rapid trade studies.

To alleviate this issue, simpler shape-based methods or feedback-driven control laws can be used to design the spiral thrust arcs as orbital transfers around the primary bodies. Shape-based low-thrust trajectory design methods usually assume tangential control direction and output the thrust levels needed to achieve the transfer [15, 16]. In the past, they have been wrapped inside stochastic solvers to determine the best solutions that satisfy practical engineering constraints [17, 18]. On the other hand, feedback control laws are pertinent for designing trajectories that constant-thrust constant-specific impulse engines can execute. These control laws use Lyapunov control theory [19, 20] or blend optimal control directions [21, 22] for each orbital element to calculate the thrust profile using knowledge of only the current and target states. The steering direction provided by blending optimal control directions is adequate for simpler problems, but Lyapunov-based control laws are usually more robust to the demands of complex transfers. Though generally suboptimal, they can be used to generate fully feasible initial guesses for higher-fidelity gradient-based optimization methods since they use significantly less computational resources and are relatively easy to implement. This also allows them to serve as good approximations for calculating the costs associated with a transfer, namely the time of flight and propellant mass consumed.

The problem of designing LELT trajectories is a challenging one due to the many revolutions required for the transfer and coordinating the use of coast arcs with the system dynamics. Existing methods of designing low-thrust low-energy (LELT) transfers are ineffective for preliminary trajectory analysis because of high computational effort and the need for successive preprocessing. This gap is critical for the planning of support and logistics for crew missions, where early-stage mission analysis tools capable of quick tradespace exploration are required. In response to this literature gap, we propose a methodology for preliminary design of low-energy low-thrust (LELT) transfers using a Lyapunov-feedback control law called Q-law within a particle swarm optimization (PSO) algorithm. We demonstrate the utility of this Q-law LELT trajectory design with PSO (QLEPSO) tool by designing a trajectory to deliver a spacecraft from a geocentric parking orbit to an Earth-moon L_1 (EML_1) halo orbit. The many-revolution thrusting phase of the transfer is approximated using Q-law, which has already been proven effective within two-body system dynamics [23, 24]. To complete the LELT transfer, the low-thrust spiral arc must be patched together with a terminal coast arc on the invariant manifold that delivers the spacecraft to the destination halo orbit. In this study, the PSO is employed to identify the ideal patch points on the manifolds, concurrently with the tunable parameters in the formulation of Q-law and the initial parking orbit. The primary objective of this paper is to develop and validate a method that can help provide rapid estimates of time-constrained low-energy low-thrust trajectories involving many revolutions. We demonstrate that the proposed method significantly improves computational efficiency while achieving near-optimal solutions.

The method developed here, designated as QLEPSO, is detailed in Section II. This procedure is then demonstrated on a selected case study in Section IV and the sample trajectories generated are validated against reference solutions available in the literature in Section V.

II. Description of QLEPSO Solution Method

The problem being considered here is that of preliminary design of minimum-fuel time-constrained low-thrust low-energy trajectories in a three-body system. The method developed here can be used to support mission design analysis, for example to seed initial guesses for more accurate trajectory analysis tools, conduct large scale trade studies, or for approximating mission costs in space logistics tools [25]. QLEPSO is specifically demonstrated on a transfer that originates at an Earth orbit and delivers the spacecraft to a halo orbit located at the Earth-moon L_1 Lagrange point (EML_1). The complete trajectory consists of two phases – the powered escape spiral to raise the spacecraft's orbit until it is delivered to the manifold, followed by a ballistic coast on the manifold, which is the low-energy pathway that leads to the desired halo orbit. The two phases are patched together at a point on the manifold surface. A stochastic optimization algorithm is then utilized to determine the ideal values of the design parameters that control the two phases, as well as the patch point itself. This algorithm uses cooperative swarm techniques to find solutions that minimize the fuel consumption while satisfying the time-of-flight constraint.

This trajectory being designed is thematically sketched in Figure 1. The process of designing the low-energy phase

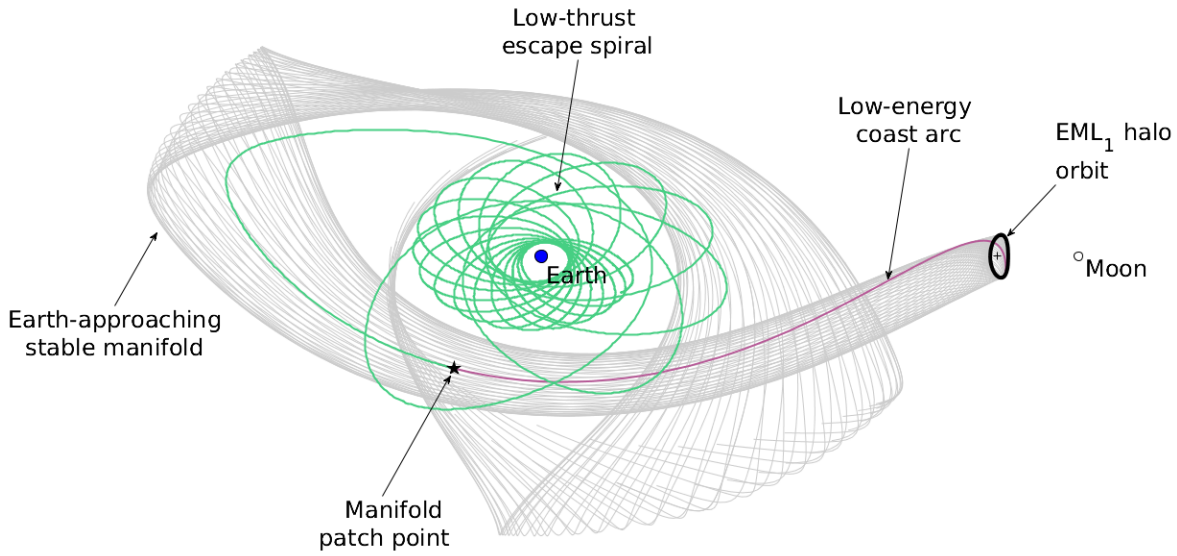

Fig. 1 Problem overview

and the low-thrust phase of the transfer is described first in this section, followed by the procedure to patch them together to yield the desired solutions.

A. Halo Orbits and Associated Invariant Manifolds for Low-Energy Transfers

The dynamics of the circular restricted three-body problem (CR3BP) are used to model the trajectory of a spacecraft in cislunar space:

$$\begin{aligned} \ddot{x} - 2\dot{y} &= \frac{\partial \Phi}{\partial x} + u_x \\ \ddot{y} + 2\dot{x} &= \frac{\partial \Phi}{\partial y} + u_y \\ \ddot{z} &= \frac{\partial \Phi}{\partial z} + u_z \end{aligned} \tag{1}$$

$$\text{where } \Phi = \frac{1}{2}(x^2 + y^2) + \frac{1-\mu}{\sqrt{(x+\mu)^2 + y^2 + z^2}} + \frac{\mu}{\sqrt{(x-(1-\mu))^2 + y^2 + z^2}}.$$

μ is the ratio of mass of the smaller primary (i.e., moon) to the sum of mass of both primaries, Φ is the potential function, and (u_x, u_y, u_z) are the components of thrust. Ballistic motion is modeled by setting the thrust components to be zero. These equations are derived in the rotating reference frame whose origin lies at the barycenter of the Earth-moon system; the units have been normalized such that angular velocity of the system, distance between the primaries and the sum of masses of the primaries are all unity.

Five points of gravitational equilibrium emerge in this system, called the Lagrange points. The three collinear Lagrange points lie one each on either side of the primaries and one in between them in the rotating frame. Linear

stability analysis of the collinear Lagrange points reveals them to be unstable, thereby giving rise to many families of unstable periodic orbits in their vicinity. Halo orbits are one such family of non-planar periodic solutions. In the current work, halo orbits of desired out-of-plane amplitude (A_z) are generated by direct transcription and collocation [12], with initial guess solutions provided by Richardson's third-order analytical approximation [26]. The manifolds can be generated by using the eigenvalues of the monodromy matrix and are time-invariant in the three-body frame. At a point along the halo orbit $\mathbf{x}(t_i)$, if the eigenvectors corresponding to the smallest and the largest real eigenvalues of the monodromy matrix are given as $\mathbf{V}^{W_s}$ and $\mathbf{V}^{W_u}$ respectively, then perturbed state at that point is given as:

$$\begin{aligned} \mathbf{X}_s &= \mathbf{x}(t_i) \pm \epsilon \mathbf{V}^{W_s} \\ \mathbf{X}_u &= \mathbf{x}(t_i) \pm \epsilon \mathbf{V}^{W_u} \end{aligned} \tag{2}$$

In this way, the states on the orbit are perturbed by a small value ϵ in the direction of the eigenvectors and propagated forward (or backward) in time using the ballistic form of Equation 1 to generate the unstable (or stable) manifold. A body of negligible mass placed on the stable manifold approaches the halo orbit asymptotically, while it can depart the same halo orbit on its unstable manifold. For certain energies of the halo orbits, these manifolds structurally resemble tubes; however, this tube-like structure is lost in regions of dynamic instabilities such as close encounters with either of the primary bodies. Each type of manifold consists of two branches, one that initially moves towards the larger primary in the system and the other that initially moves away from it. In this paper, we concentrate on designing transfers from Earth to halo orbits and hence focus on the Earth-approaching branch of the stable manifold.

Every point on the manifold structure can be parametrized using two values – point of origin of the corresponding manifold trajectory on the halo orbit, τ_h, and time to reach the halo once on that manifold, τ_m. The halo orbit insertion parameter (τ_h) represents the normalized position around the periodic orbit with respect to the point where the maximum out-of-plane amplitude is achieved. The manifold insertion parameter (τ_m), on the other hand, is time propagated to arrive at the given point on the manifold. The direction of propagation is forward in time for the case of the unstable manifold, and backward for generating the stable manifold.

B. Feedback Control Law for Low-Thrust Orbital Transfers

Q-law is a Lyapunov feedback control law developed by Petropoulos [20, 27] for designing low-thrust orbital transfers around a primary body. Based on Gauss variational equations, it decides the thrust direction at any point during the trajectory based on the "remaining distance to go" and can target defined changes in all orbital elements except true anomaly. Q-law has been previously used successfully to provide good initial guesses for optimal transfers [23, 28] using constant specific impulse, constant thrust engines in a two-body system model. It provides a non-iterative alternative to calculating a low-thrust transfer between arbitrary orbits, thereby providing a computationally efficient

control law.

The basis of calculating these transfers is the following proximity quotient Q, a candidate Lyapunov function that quantifies the proximity of the current orbit to the target orbit [20]:

$$Q = \left(1 + W_p P\right) \sum_{\varpi} W_{\varpi} S_{\varpi} \left[\frac{d(\varpi, \varpi_T)}{\dot{\varpi}_{xx}}\right]^2 \tag{3}$$

where ϖ denotes the instantaneous values of the orbital elements being targeted and the subscript T denotes their target values. W_p and W_{ϖ} are scalar weights such that W_{ϖ} is non-zero for those elements being targeted and W_p is non-zero when enforcing a minimum periapse condition using the penalty function P. S_{ϖ} is the scaling function and $d(\varpi, \varpi_T)$ is the distance function, which denotes the difference between current and target orbital elements pertinent in the current case. In the implementation within this paper, no minimum periapse condition is enforced (i.e., $W_p = 0$ and thus P is omitted). On the other hand, the scaling function S_{ϖ} is chosen as suggested by the original Q-law formulation to aid in convergence of the semi-major axis to its target value:

$$S_{\varpi} = \begin{cases} \left[1 + \left(\dfrac{a - a_T}{3a_T}\right)^4\right]^{\frac{1}{2}} & \text{for } \varpi = a \\ 1 & \text{for } \varpi = e, i \end{cases} \tag{4}$$

The term $\dot{\varpi}_{xx}$ in Equation 3 denotes the maximum rate of change of orbital element due to thrust over thrust direction and over true anomaly. Analytic expressions for it are derived by using the Gauss variational equations (below). If the perturbing acceleration $\mathbf{f}$ is given by its components (f_r, f_θ, f_h) in the radial, circumferential and angular momentum directions respectively, then:

$$\begin{aligned} \frac{da}{dt} &= \frac{2a^2}{h}\left(e \sin\theta f_r + \frac{p}{r} f_\theta\right) \\ \frac{de}{dt} &= \frac{1}{h}\left\{p \sin\theta f_r + [(p + r)\cos\theta + re] f_\theta\right\} \\ \frac{di}{dt} &= \frac{r\cos(\theta + \omega)}{h} f_h \\ \frac{d\Omega}{dt} &= \frac{r \sin(\theta + \omega)}{h \sin i} f_h \\ \frac{d\omega}{dt} &= \frac{1}{eh}\left\{-p\cos\theta f_r + (p + r)\sin\theta f_\theta\right\} - \frac{r \sin(\theta + \omega)\cos i}{h \sin i} f_h \\ \frac{d\theta}{dt} &= \frac{h}{r^2} + \frac{1}{eh}\left\{p\cos\theta f_r - (p + r)\sin\theta f_\theta\right\} \end{aligned} \tag{5}$$

where t = time, p = semilatus rectum, h = angular momentum of the orbit, and r = radius from the central body =

$p/(1 + e\cos\theta)$. By representing the vector of orbital elements as $\mathbf{X}$, the above equations can be reduced to this form:

$$\dot{\mathbf{X}} = \mathbf{\Psi}(\mathbf{X}) \cdot \mathbf{f} \tag{6}$$

The perturbing acceleration $\mathbf{f}$ consists of the thrust provided by the spacecraft as well as the third-body gravitational perturbation by the moon. However, only acceleration provided by the low-thrust engine is included for the purpose of deriving the expressions for $\dot{\alpha}_{xx}$, and thus the Lyapunov-optimal control. If T = thrust provided by the engines, m = mass of the spacecraft, α = in-plane thrusting angle and β = out-of-plane thrusting angle, then the vector $\mathbf{f}^{LT}$ representing the control acceleration vector provided by the low-thrust engines, specified by its components $(f_r^{LT}, f_\theta^{LT}, f_h^{LT})$, is:

$$\begin{aligned} f_r^{LT} &= f^{LT} \cos\beta \sin\alpha \\ f_\theta^{LT} &= f^{LT} \cos\beta \cos\alpha \\ f_h^{LT} &= f^{LT} \sin\beta \end{aligned} \tag{7}$$

where $f^{LT} = |\mathbf{f}^{LT}| = \dfrac{T}{m}$. By setting $\dot{\alpha}_{xx} = \max\limits_{\alpha,\beta,\theta} \dot{\alpha}$ with $\mathbf{f} = \mathbf{f}^{LT}$, the corresponding terms in the expression for Q can be obtained from Equation 5 as:

$$\begin{aligned} \dot{a}_{xx} &= 2f^{LT}\sqrt{\frac{a^3(1+e)}{\mu(1-e)}} \\ \dot{e}_{xx} &= \frac{2pf^{LT}}{h} \\ \dot{i}_{xx} &= \frac{pf^{LT}}{h\left(\sqrt{1-e^2\sin^2\omega} - e|\cos\omega|\right)} \end{aligned} \tag{8}$$

The proximity quotient Q in Equation 3 is now fully defined. Its value is zero at the target orbit and positive along the transfer trajectory. The thrust direction at any instant along the transfer is calculated such that the proximity quotient is driven to zero as quickly as possible, i.e., the direction in which $\dot{Q}$ attains its most negative value. By applying Lyapunov control theory, the instantaneous optimal control vector can be derived using the notation in Equation 6 as:

$$\mathbf{f}^{LT} = -\mathbf{\Psi}^T \left(\frac{\partial Q}{\partial \mathbf{X}}\right)^T \tag{9}$$

Symbolic differentiation was employed at this juncture to determine the Q-law control expressions.

Although the Lyapunov-optimal control in the above equation is derived without considering third-body perturbing forces, the effect is included while propagating the system equations (Equation 5). Gravitational perturbations due to the effect of the moon are dominant in this problem and the angular position of the moon in the Earth-fixed frame (λ) is

appended to the system equations for state propagation as:

$$\frac{d\lambda}{dt} = n^{\,\mathbb{D}} \tag{10}$$

where $n^{\,\mathbb{D}}$ is the mean motion of the moon as it orbits the Earth. The perturbing acceleration in Equation 5 becomes:

$$\mathbf{f} = \mathbf{f}^{LT} + \mathbf{f}^{\,\mathbb{D}} \tag{11}$$
$$\text{where } \mathbf{f}^{\,\mathbb{D}} = \mu^{\,\mathbb{D}} \left(\frac{\mathbf{r}^{\,\mathbb{D}} - \mathbf{r}}{|\mathbf{r}^{\,\mathbb{D}} - \mathbf{r}|^3} - \frac{\mathbf{r}^{\,\mathbb{D}}}{|\mathbf{r}^{\,\mathbb{D}}|^3} \right)$$

The components of $\mathbf{r}$ (spacecraft position vector) and $\mathbf{r}^{\,\mathbb{D}}$ (position vector of the moon) in the radial, circumferential and angular momentum directions are as follows and are meant for substitution into Equation 11:

$$\begin{aligned} r_r^{\,\mathbb{D}} &= a^{\,\mathbb{D}} \left[\cos\theta\cos(\lambda^{\,\mathbb{D}} - \Omega) + \cos i \sin\theta \sin(\lambda^{\,\mathbb{D}} - \Omega)\right] && r_r = r \\ r_\theta^{\,\mathbb{D}} &= a^{\,\mathbb{D}} \left[-\sin\theta\cos(\lambda^{\,\mathbb{D}} - \Omega) + \cos i \cos\theta \sin(\lambda^{\,\mathbb{D}} - \Omega)\right] && r_\theta = 0 \\ r_h^{\,\mathbb{D}} &= a^{\,\mathbb{D}} \left[-\sin i \sin(\lambda^{\,\mathbb{D}} - \Omega)\right] && r_h = 0 \end{aligned} \tag{12}$$

The mass of the spacecraft is also tracked along the trajectory, through the following equation:

$$\frac{dm}{dt} = \frac{-T}{g I_{sp}} \tag{13}$$

where g = standard acceleration due to gravity and I_{sp} = specific impulse imparted by the low-thrust engine.

To reiterate, the current Q-law implementation calculates the optimal thrust direction without accounting for the third-body perturbations, but they are indeed included during system propagation. The algorithm also implements fixed-step integration as prescribed in the original work [27]. Additionally, the mechanism for coasting available within the original Q-law is implemented to allow thrusting during portions of the trajectory where it is most effective to do so. The absolute effectivity at any true anomaly is given as:

$$\eta_a = \frac{\dot{Q}_n}{\dot{Q}_{nn}} \tag{14}$$

where $\dot{Q}_n = \min_{\alpha,\beta} \dot{Q}$ and $\dot{Q}_{nn} = \min_{\theta} \dot{Q}_n$. A cut-off value η_{cut}, can be chosen for this parameter to prevent the spacecraft from thrusting if the value of absolute effectivity is below η_{cut}. This parameter, in effect, manages the extent of coasting during the transfer phase governed by this control law. In addition to this mechanism for controlling coasting periods, the effect of eclipse periods can also be included as unplanned shut-offs, though not implemented here.

Although Lyapunov methods have no guarantee of convergence, Q-law has been empirically shown to converge to the target orbit for a broad range of orbital transfers [27]. It has also been shown to provide rapid and acceptable estimates of the trajectory behavior and the performance costs of orbital transfers within a two-body perspective [29]. In this paper, this same feedback control law is applied in a three-body system to design the powered section of the trajectory that connects to the low-energy pathway. The complete process is described in Section II.C.

C. Complete LELT Trajectory Design

By breaking down the desired LELT trajectories as orbital transfers around the primary body (Earth), with the stable manifold providing "free" transport to the destination three-body periodic orbit, Q-law can be applied here to design the escape spiral. As an example to demonstrate this strategy, consider a trajectory from an initial Earth parking orbit to an EML_1 halo orbit. The spacecraft must be delivered to the stable manifold for a ballistic transfer to the corresponding halo orbit. Once the manifold is generated, all the points on this manifold are considered viable targets for the low-thrust arc. The equivalent classical orbital representation of these target points is found by converting the coordinates from the Earth-moon rotating frame to an Earth-centered inertial frame. These candidate patch points have fixed true anomalies and so, Q-law has to be propagated backwards in time starting from the final manifold location (i.e., the patch point) and ending at initial parking orbit. A complete LELT trajectory can be designed in this manner for each point on the manifold. This trajectory is refined by use of advantageous values for decision variables, selected by a stochastic particle swarm optimization (PSO) algorithm. The complete procedure to design the Q-law LELT trajectories using a PSO, dubbed QLEPSO for brevity, is summarized in Figure 2.

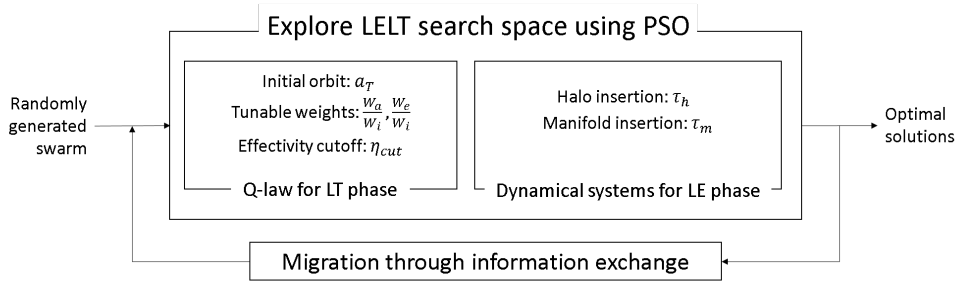

Fig. 2 Overview of the QLEPSO method

1. Cost Function

The LELT trajectories being designed here will consist of two phases connected with each other at the manifold patch point – the orbit raising phase consisting of many revolutions around the Earth, and the final coast arc on the manifold that asymptotically brings the spacecraft to the halo orbit. The objective for this complete LELT trajectory is to minimize the propellant mass consumed. Reduction in consumed propellant mass is typically obtained at the cost of higher time of flight (TOF) in low-thrust trajectory solutions. Thus, the transfers in this study are sought for fixed

flight times, where the flight time includes the intermittently powered escape spiral as well as the ballistic coast on the manifold. Mathematically, this optimization problem can be stated as:

$$\begin{aligned} \underset{\mathbf{x}}{\text{minimize}} \quad & J(\mathbf{x}) = m_{propellant} \\ \text{subject to} \quad & \mathbf{f}(\mathbf{x}) \leq \mathbf{b_C} \\ & \mathbf{b_L} \leq \mathbf{x} \leq \mathbf{b_U}, \\ \text{where} \quad & \mathbf{x} = \left[a_T,\ \frac{W_a}{W_i},\ \frac{W_e}{W_i}, \eta_{cut},\ \tau_h,\ \tau_m, \right]^T. \end{aligned} \tag{15}$$

This problem is restricted by two constraints, one regarding the initial parking orbit and the other relating to the allowable maximum time of flight. Additionally, the decision variables are also subject to bounds. These constraints ($\mathbf{f}(\mathbf{x})$ and $\mathbf{b_C}$) and the problem bounds ($\mathbf{b_U}$ and $\mathbf{b_L}$) are described in detail after introducing the decision variables.

2. Decision Variables

The decision vector $\mathbf{x}$ is comprised of variables that determine the cost of the transfer. Within the described LELT trajectory design strategy, values of the following variables can be judiciously selected to construct cheaper transfers:

1) Parking orbit specification $\rightarrow a_T$
2) Variables in Q-law computations $\rightarrow \frac{W_a}{W_i}$, $\frac{W_e}{W_i}$ and η_{cut}
3) Manifold patch point selection $\rightarrow \tau_h$ and τ_m

Following the trajectory in its temporal order, the first parameter that can be optimized is the parking orbit from which the spacecraft begins its journey. The two common launch orbits are the low Earth orbit (LEO) and the geosynchronous transfer orbit (GTO), which is used to deliver satellites to their operational geosynchronous Earth orbit (GEO). Although some previous LELT trajectory design studies have selected the GTO as the initial parking orbit [7, 12], some benefit could be realized by optimizing this orbit itself. The search space for this initial parking orbit is limited in the current study by the Δv that can be imparted by the launch vehicle, which differentiates it from the analysis in previous works such as [9] and [10]. This available Δv is calculated by fixing the perigee at LEO altitude and then calculating the single impulsive maneuver required to raise the orbit from LEO to GTO (with no inclination change):

$$\Delta \mathrm{v}_{\mathrm{budget}} = v_p^{\mathrm{GTO}} - v_p^{\mathrm{LEO}} \tag{16}$$

The subscript p denotes perigee in the above equation. Given this Δv budget after launch, two parameters can be changed: the apogee and the inclination of the initial parking orbit for the LELT journey. This Δv can be distributed optimally between increasing the semi-major axis and changing the inclination of the parking orbit, such that the residual changes required to reach the manifold can be executed by the low-thrust phase of the trajectory. However, since the

semi-major axis and inclination of the parking orbit that can be achieved in this manner is constrained by the Δv budget considered earlier, only one of them needs to be a decision variable. Assuming that a *single* maneuver conducted at perigee places the spacecraft into its parking orbit, this constraint can be expressed as:

$$\Delta \mathrm{v}_{\mathrm{budget}} = \sqrt{\left(v_p^{\mathrm{park}}\right)^2 + \left(v_p^{\mathrm{LEO}}\right)^2 - 2v_p^{\mathrm{park}} v_p^{\mathrm{LEO}} \cos \Delta i} \tag{17}$$
$$\text{where } \; v_{\mathrm{p}}^{\mathrm{park}} = \sqrt{\mu_\oplus \left(\frac{2}{r_p} - \frac{1}{a_T}\right)}$$

Thus, the selection of the parking orbit can be completely parametrized by its semi-major axis a_T. This is possible due to the assumption that the parking orbit is achieved by a single impulse after launch. If multiple impulses are allowed, additional parameters may be included in the decision vector to match the new problem structure.

Consequent to determination of the Earth parking orbit, the low-thrust phase of the transfer is calculated using Q-law. Only three orbital elements of the parking orbit are targeted – semi-major axis (a), eccentricity (e) and inclination (i) – and so only three weights (W_a, W_e, W_i) need to be specified. The other secular elements of the initial parking orbit (i.e., ω and Ω) are only incidentally chosen by the optimal solutions and can be matched by adjusting the time frame of the spacecraft launch or its insertion into the parking orbit. The low-thrust phase can be optimized by tuning the weights of Q-law by using the relative values of W_a, W_e and W_i in the form of W_a/W_i and W_e/W_i, as well as the value of η_{cut}. The coefficients in the original formulation of the scaling function S_{oe} in Equation 4 (refer [20, 27]) could also be included in the decision vector; however, sensitivity of the low-thrust trajectory to these parameters has been shown to be negligible [24].

The final optimization variables select the manifold patch point that separates the powered section of the trajectory from the purely ballistic portion. It is parametrized by the halo orbit insertion parameter τ_h and the manifold insertion parameter τ_m. As explained before, τ_h is the normalized position; the value of zero (and one due to periodicity) commonly indicates the point at which the halo orbit achieves its maximum value along the positive Z-axis. Similarly, τ_m is typically specified in normalized time units (in the Earth-moon rotating / synodic frame). In order to clearly indicate the direction of propagation, τ_m is negative for the stable manifold and positive for the unstable manifold. Once the spacecraft is inserted onto the manifold at the patch point specified by τ_m and τ_h, it travels ballistically to the desired halo and completes the transfer.

3. Constraints

Given this solution approach, the optimization problem in Equation 15 is subject to certain constraints and bounds. The first constraint regards the relationship between the decision variable a_T and other parameters that definitively

specify the initial parking orbit through the Δv budget. Combining Equations 16-17, the constraint translates to:

$$\begin{gathered} f_1(\mathbf{x}) = b_{C_1} \\ \text{where} \quad f_1(\mathbf{x}) = f(a_T) = \sqrt{(v_p^{\text{park}})^2 + (v_p^{\text{LEO}})^2 - 2v_p^{\text{park}} v_p^{\text{LEO}} \cos \Delta i} \\ \text{and} \quad b_{C_1} = \Delta \text{v}_{\text{budget}} = v_p^{\text{GTO}} - v_p^{\text{LEO}}. \end{gathered} \tag{18}$$

The underlying assumption here is that the entire budget available to the launch vehicle is exhausted in achieving the parking orbit, prior to commencing the low-thrust phase. This allows for a more equitable calculation of propellant mass consumed in different candidate solutions. The second constraint considers the time of flight restriction and is expressed as:

$$\begin{gathered} f_2(\mathbf{x}) \leq b_{C_2} \\ \text{where} \quad f_2(\mathbf{x}) = g_{\text{Q-law}} \left(a_T, \frac{W_a}{W_i}, \frac{W_e}{W_i}, \eta_{cut} \right) + |\tau_m| \\ \text{and} \quad b_{C_2} = \text{TOF}_{max}. \end{gathered} \tag{19}$$

The function $g_{\text{Q-law}}$ produces the time of flight required to complete the orbit raising spiral and is calculated simultaneously as the objective function (i.e., $\Delta m_{propellant}$) by using Q-law. The time spent coasting on the manifold in order to complete the second phase of the transfer is simply equal to the absolute value of τ_m. This τ_m takes a negative value when used to parameterize the stable manifold because the stable manifold is obtained by propagating the CR3BP system equations backward in time. In addition to these constraints, the search space of the decision variables is restricted by means of upper and lower bounds. These bounds are problem specific and their selection for the current sample case is outlined in Section III.

4. Selection of Optimization Algorithm for LELT Trajectory Design

In previous work, the search space was confined to two decision variables (τ_h and τ_m) and hence was amenable to a straightforward grid search [30]. However, within the current problem setup, the search space is composed of six dimensions and thus attempting all configurations is computationally challenging. Stochastic optimization algorithms are well suited to explore the solution space for the current problem in an automated manner without much guidance from the user. In previous works that investigated the applications of different stochastic optimization techniques, the general consensus is that the choice must align with the problem structure for effectiveness. In the current work, we have chosen the particle swarm algorithm due to its compatibility with the current problem structure where the search space associated with each of the decision variables is continuous, as well as its higher speed of convergence* [31].

*vs. differential evolution and simulated annealing, when applied to a general class of benchmark problems

Although the PSO is chosen in this work, it is expected that other algorithms such as differential evolution can also be applied successfully.

The PSO algorithm, originally introduced by Kennedy and Eberhart [32], is driven by cooperation between particles in a swarm by exchange of information about the best-found-solutions. This guides the motion of the initial population towards the optimal point. Beginning with a randomly generated initial random swarm of N particles, $\mathbf{x}_j^0$ where $j = 1, 2, ...N$, the new position of the particle j at the $(k+1)^{\text{th}}$ iteration is calculated as:

$$\begin{aligned} \mathbf{x}_j^{k+1} &= \mathbf{x}_j^k + \mathbf{v}_j^{k+1} \\ \text{where } \mathbf{v}_j^{k+1} &= C_i \mathbf{v}_j^k + C_c R_1 (\mathbf{p}_j - \mathbf{x}_j^k) + C_s R_2 (\mathbf{g}^k - \mathbf{x}_j^k) \end{aligned} \tag{20}$$

The constants C_i, C_c and C_s are the inertial, cognitive and social weighting coefficients respectively. The fitness of all particles is evaluated at each iteration to determine the best position of each particle over time, $\mathbf{p}_j$, and the best global value in the current swarm, $\mathbf{g}^k$. R_1 and R_2 are randomly generated numbers that lie between 0 and 1, selected from a uniform distribution. If a particle strays outside the specified boundary, the algorithm handles it by setting those components equal to the corresponding bound. The algorithm terminates either when maximum number of iterations N_{IT} is reached, or when the solution has not improved (i.e., has stalled) for N_{ST} iterations.

5. Method of Treating Constraints

Two constraints are present in the current problem (Equation 15-19). Constraints can be treated within the PSO algorithm using the "penalty" method [33, 34], where penalties commensurate with the constraint violations are added to the candidate's fitness function evaluation. However, finding ways to reduce complexity of implementation by exploiting problem structure can benefit the computational resource consumption.

In the problem under consideration, the first constraint is a linear equality that deals with controlling the initial parking orbit where the low-thrust journey begins. Due to the structure of the problem, the linear equality constraint in Equation 18 can be interpreted as placing bounds on the value of a_T instead. Its lower bound is set at $a_T = a_{\text{LEO}}$, which corresponds to the limiting case where the launch vehicle expends its entire budget to make only an inclination change. The upper bound is calculated in an opposite manner by setting $\Delta i = 0$ in Equation 17, resulting in $a_T = a_{\text{GTO}}$. This implementation allows the use of the simpler unconstrained (but bounded) versions of optimization algorithms in the absence of any other constraints.

On the other hand, the inequality constraint in Equation 19 restricts the time of flight. Two methods were considered here to handle this constraint, (1) the previously mentioned penalty method, (2) a simple strategy of assigning a fictitious high cost to infeasible candidate solutions (similar to the strategy used in [35] to treat inequality constraints). In trials, the constrained optimization method by employing penalties to feasibilize candidates (method #1) converged to final

solutions in less number of iterations than the second strategy. However, the overall computational runtime was longer because the optimizer needs to evaluate very long (infeasible) Q-law flight time solutions during the optimization. The simpler approach (method #2) worked well during the course of this work due to low computational runtimes from bounding the Q-law flight times. Candidate solutions that exceed the time of flight constraint are simply marked within the fitness function to consume all of the available mass.

III. Problem Setup for Case Study

The LELT trajectory design process described in this paper is demonstrated on a transfer that starts at a geocentric parking orbit and delivers the spacecraft to an EML_1 halo orbit. The PSO algorithm used in this work is the native `particleswarm` available in MATLAB [36]. Progression of this algorithm can be controlled by setting different values for C_c, C_i and C_s, as used in Equation 20 for updating velocity of particles at each iteration. The values used in this study are charted out in Table 1, along with the conditions for terminating the PSO run. All requisite integration is conducted in corresponding nondimensionalized units within the cost function, with the intent of properly scaling and conditioning the numerical integration process. Three-body (CR3BP) nondimensional units are used for halo and manifold generation (where 1DU = distance between Earth and moon), and two-body nondimensional units used within Q-law implementation (where 1DU = Earth radius).

Table 1 PSO algorithm parameters

Parameter	Value
Inertial weight C_i	[0.1, 1.1]
Cognitive weight C_c	1.49
Social weight C_s	1.49
Number of particles N	200
Maximum number of iterations allowed N_{IT}	200
Number of stall iterations allowed N_{ST}	20

Table 2 Q-law algorithm parameters

Parameter	Value
Fixed time step	1000 s
Integration scheme	RK6 [37]
Target convergence radius for a	10 km
Target convergence radius for e	0.005
Target convergence radius for i	0.005 rad
Weight on inclination change W_i	1

The LELT trajectory is assembled using the values of decision variables selected by the PSO. The low-thrust engine used to affect this trajectory is assumed to provide a constant thrust of 0.7 N and a fixed specific impulse of 3000 s. The final mass delivered to the halo orbit is fixed at 1000 kg. This means that the spacecraft's *final* thrust acceleration is 7×10^{-4}m/s^2. The low-thrust trajectory is designed using the Q-law algorithm with the parameters specified in Table 2. No minimum periapse constraint is enforced and so W_p is set to zero.

The PSO algorithm also requires definition of the search space with respect to each component of the decision vector ($\mathbf{x}$ in Equation 15). In order to do so, suitable bounds are defined on each decision variable as specified in Table 3. These bounds are either derived from the problem structure or assumed so as to confine the search space to a finite region. The first decision variable is the semi-major axis of the initial Earth parking orbit (a_T). Its perigee altitude (h_p) is fixed at

Table 3 Bounds on decision variables

Parameter	Lower bound	Upper bound
a_T	6563 km	24510 km
W_a/W_i	0.001	1000
W_e/W_i	0.001	1000
η_{cut}	0	0.5
τ_h	0	1
τ_m	-3π TU	-1π TU

400 km, while its apogee and inclination are free to vary. These two parameters are however constrained by a Δv budget equal to that required for a transfer between LEO and a GTO-sized orbit at perigee with an impulsive maneuver:

$$\Delta v_{\text{budget}} = v_p^{\text{GTO}} - v_p^{\text{LEO}} = 2.3988 \text{ km/s} \tag{21}$$

Once the optimizer (i.e. the PSO) selects the semi-major axis a_T of the parking orbit, then its inclination can be calculated by substituting the above Δv_{budget} in Equation 17. In the current implementation, this constraint is instead expressed as a bound on a_T as in Table 3 – the lower bound is set at the orbital size that can be achieved is the entire Δv budget is used to change inclination (i.e., lower bound set at LEO), while the upper bound is set where the available budget is used completely for apogee raising only (i.e., GTO). As described earlier, this calculation is based on the assumption that this Δv budget is completely consumed to reach the parking orbit.

Table 4 GTO and GEO specifications

Parameter	GTO	GEO
Semi-major axis a	24510 km	42164 km
Eccentricity e	0.7234	0.005 †
Inclination i	23.43°	23.43°
Argument of periapse ω	Free	Free
Longitude of ascending node Ω	Free	Free

Table 5 EML_1 halo orbit specifications

Parameter	Value
Amplitude A_z	+8000 km
Type	Northern
Period	11.924 days
Initial position	[0.823383, 0, 0.020812] DU
Initial velocity	[0, 0.133228, 0] DU/TU

The inclination of the parking orbit is expressed with respect to the Earth-moon plane. When the parking orbit is allowed to vary freely, the angular separation from the nominally-inclined LEO imparted by the launch vehicle depends on the how of its fuel budget was consumed for raising the apogee. In certain comparative cases of later sections, the parking orbit is fixed at geosynchronous transfer orbit (GTO) (Table 4) in order to match conditions of the past studies. Assuming that the GTO lies in the Earth's equatorial plane, its specified inclination reflects the mean angular separation between the Earth's equatorial plane and the plane of the moon's orbit. The angular separation of these two planes varies between 18.28° and 28.58° [38]. Similarly, the GEO specifications are defined in Table 4 for later use. However,

† Nominal non-zero value specified to avoid singularity in Gauss variational equations

for the sample case used for demonstration of the method, the inclination is allowed to freely vary within the Δv_{budget} constraint as explained earlier.

Once the parking orbit is selected, the Q-law computations can begin. The next two variables in the decision vector are related to the performance of Q-law and control the rates at which the semi-major axis and eccentricity converge to their target values with respect to the convergence speed of inclination to its target value. Instead of focusing on the absolute values of these variables, it is sufficient to find their relative values, thereby controlling the relative magnitudes of the components of the instantaneous control vector. Reasonable bounds are chosen for these variables. The fourth decision variable (η_{cut}) decides the placement and duration of coast arcs within the escape spiral and its lower bound is set to zero (i.e. continuous thrust escape spiral with no coasting). While the natural upper bound on this effectivity cutoff approaches unity (which involves a coast-only trajectory with TOF approaching infinity), the upper bound is set to 0.5 instead. This educated estimate improves the convergence properties of the PSO by guiding it to a feasible region faster.

The EML_1 halo orbit used in this work follows the specifications presented in Table 5. A perturbation ϵ of 5 km (Equation 2) is used to generate the Earth-approaching branch of the stable manifold. It is propagated backwards in time for 3π normalized time units (synodic TU), a time span that converts to little more than 40 days. The manifold surface exposed for selection of insertion points covers at least two closest approaches to Earth and the solution space is thus deemed large enough for practical engineering purposes. This setup decides the bounds on the last two decision variables. The penultimate variable τ_h (halo orbit insertion parameter) is already normalized and bound between 0 and 1. Since the values of the final decision variable, τ_m, are negative for the stable manifold, the lower bound on τ_m is the time at which the (backward) integration of the manifold is terminated (-3π here). The upper bound is placed where all the manifolds have approximately departed the lunar sphere of influence (SOI), which is approximately $-\pi$ in this case. The radius of this SOI, centered at the moon, is calculated as [39]:

$$r_{SOI} \approx a_{\leftmoon} \left(\frac{m_{\leftmoon}}{m_{\oplus}} \right)^{\frac{2}{5}} = 66183.85\text{km}.$$

The part of the manifold surface of interest in this sample problem is the section that lies beyond the lunar SOI; this represents the low-energy search space for the current case study. These bounds on τ_m represent the region where Q-law is effective, because it is derived using the two-body equations of motion (lunar gravity is added as third-body gravitational perturbation during propagation only). Within the boundaries of the lunar SOI, the derived equations will still produce feasible solutions even though the control directions dictated by Q-law would be less effective. This case is simulated in a later section in order to compare QLEPSO results with those found in the literature, where control dictated by Q-law is used for direct delivery to the halo orbit even though the spacecraft's state places it inside this lunar sphere of influence.

Although the current sample case handles LELT transfer to the EML_1 halo, the use of this lunar SOI also aids

design of transfers to EML_2 halo orbits, whose Earth-approaching stable manifold branch crosses the moon first. In the absence of this bound on τ_m, using the QLEPSO method to design such transfers may otherwise involve using Q-law derived in the Earth-centered frame too close to the moon. Additionally, such transfers would require stricter bounds to be derived and used on the variable τ_h because certain sections of the manifold surface originating at EML_2 halo orbits do not approach Earth after their lunar flyby.

IV. Results

The PSO algorithm is run for six trials with 200 particles and the optimization results are organized in Table 6. For these runs, the total TOF is constrained to be less than or equal to 90 days. This value of maximum TOF is chosen so as to simplify the process of comparison with results from independent past studies in later sections. The stochastic nature of particle swarm optimization gives rise to variance in the results presented by each run. Table 6 summarizes the results from five identical trial runs of the PSO, beginning with randomly distributed particle positions and velocities. This table proves that the variance of results is within a narrow range and hence acceptable.

Table 6 QLEPSO results for total TOF ≤ 90 days

Parameter	Run #1	Run #2	Run #3	Run #4	Run #5
			Raw values of decision variables		
a_T, km	24294.2907	24282.4559	24290.4436	24375.4808	24311.8243
W_a/W_i	588.4616	636.6509	830.1153	89.4069	212.4609
W_e/W_i	814.2662	836.2408	946.7234	122.6418	296.5848
η_{cut}	0.0771	0.0743	0.0668	0.0764	0.0773
τ_h	0.7343	0.7245	0.7377	0.7441	0.7335
τ_m, synodic TU	-1.000π	-1.002π	-1.0043π	-1.0017π	-1.000π
			Qualitative properties of solutions		
Orbit raising TOF, days	76.3542	76.3542	76.2847	76.3310	76.3426
Manifold coast TOF, days	13.6427	13.6456	13.7014	13.6657	13.6432
Mass fraction consumed, %	7.7708	7.7769	7.7911	7.7607	7.7688

Some useful insights can be gathered from the results in Table 6. Tracing the trajectory again in its temporal order of phases, the results show that almost the entire Δv budget available to the launch vehicle is used to raise its initial parking orbit to the size of GTO, keeping its inclination (with respect to the Earth-moon plane) close to zero. This can be explained by two intuitive causes: (1) the inclination of all the points on the manifold surface lies within 3° of the Earth-moon plane, and (2) the low-thrust trajectory may be able to better satisfy the constraint on the flight time by starting at the parking orbit with the highest permitted apogee. Thus the optimal parking orbit chosen represents the upper limit placed on the a_T variable; this observation is consistent with that made by Kluever [40] when designing combined chemical-electric transfers to GEO.

The other noticeable feature is the range of values of the Q-law weights exhibited in the five runs; however, the ratio of W_a/W_i to W_e/W_i remains approximately constant ($\approx 0.7 - 0.8$). This can be explained by the Q-law formulation where the three components of the thrust vector are decided by the relative (not absolute) values of the weights. The trajectory corresponding to fourth trial run is presented in Figure 3. The regions that the Q-law decides to coast (within the escape spiral) are noticeable and occur at the apogees. The length of the manifold coast arc is minimal and the spiral escape arc seen to deliver the spacecraft very close to the halo orbit.

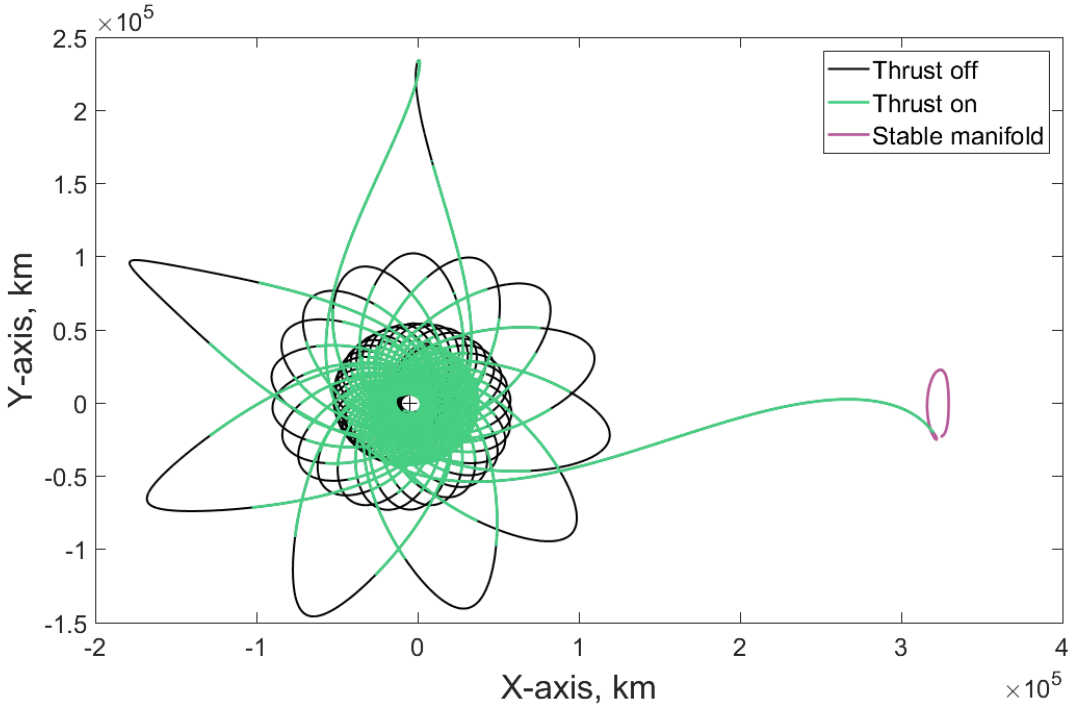

Fig. 3 Complete trajectory to best patch point found using QLEPSO

Another prominent feature of the QLEPSO solutions is the consistent selection of the lowest allowed value of τ_m (refer Table 3), which identifies the portion of the journey spent coasting on the manifold. By minimizing the length of this manifold coast arc, the optimizer seeks to maximize the amount of coasting allowed within orbit raising portion of the transfer. These results are in contrast with a separate study that conducted LELT trajectory design using Q-law [41], where an attempt to enable large-scale tradespace exploration was made by heuristically deriving the optimal manifold patch point. This metric, referred to as Q_p, consisted of weighted sum of relative "distance" between a point on the halo orbit's manifold and the Earth parking orbit. The manner of selecting patch points with low values of Q_p reflects the fundamental directive of Q-law to reduce the distance between the starting and destination orbits. As a general trend, this Q_p reduced in value as the stable manifold was propagated farther backwards in time; thus, the points on the section of the manifold surface far away from the halo orbit were selected as patch points. In the referenced study, the physical neighborhood of the heuristically chosen manifold patch point was then iteratively explored in order to find solutions

that satisfied a given time-of-flight constraint. The Q-law weights were set to unity for this purpose. However, the results from the current analysis imply that delivering the spacecraft as close to the halo orbit as allowable is the optimal strategy when constraining the total time of flight. This allows the orbit-raising spiral arc to consume the majority of the coasting budget, thereby naturally reducing the propellant consumed for the transfer by leveraging the orbital dynamics instead. Though the analysis in [41] was conducted for transfer to an EML_2 halo orbit and the results here pertain to EML_1 halo orbit, similar reasoning is expected to apply. Thus, the patch point that separates the low-thrust phase and the low-energy phase must be chosen with care and the current method can effectively do so, as shown by the trend within the optimal QLEPSO constrained-TOF solutions to pick manifold patch points close to the target halo orbit.

V. Comparison with Reference Methods/Solutions

In this section, the results from the QLEPSO method developed here are compared with reference methods/solutions to quantify its accuracy for designing low-energy low-thrust transfers in the three-body system. Available methods in the literature have used different techniques to design LELT trajectories. Here, QLEPSO is first compared with other heuristic methods available in the literature and then with solutions obtained using deterministic gradient-based methods.

A. Use of Tangential Thrust for Orbit Raising Arc

The first reference study chosen is provided by Abraham et.al. [42] where a method for preliminary mission analysis was developed and used to design a transfer from a GEO-energy orbit to a large-amplitude halo orbit. In this reference, the LELT trajectory is similarly constructed using a PSO, with the exception of the control law used to design the low-thrust phase. The escape spiral in [42] instead employs tangential control, where thrust acceleration is applied in the opposite direction as the spacecraft's velocity in the CR3BP frame. Beginning at the manifold patch point, this escape spiral is propagated backward using three-body dynamics (Equation 1) until an orbit matching the energy of GEO is achieved. The following cost function was used in [42] within a local PSO to determine solutions where the terminating GEO-energy orbit is also circular:

$$J_{abraham} = k_1(e_{terminate} - e_{desired}) + k_2\Delta T + k_3\Delta m \tag{22}$$

where ΔT is the total time of flight and Δm is the propellant consumed. $e_{terminate}$ is the osculating eccentricity at the termination of the backward propagated thrust arc, while its desired value, $e_{desired}$, is zero (i.e., eccentricity of GEO). A process for selecting values of the constants k_1, k_2, k_3 depending on the expected values of the three terms in the cost function is detailed in the original work. The values used here are $k_1 = 1$, $k_2 = 0.002$ and $k_3 = 0.001$.

For this analysis, the QLEPSO method outlined here, as well as the tangential thrust method, is applied first to the

halo orbit chosen in [42] (EML$_1$ A_z≈72000km). First off, the method in the reference is replicated and tangential control law is used for the orbit raising spiral. Next, the same transfer is calculated using Q-law, where the GEO specified in Table 4 is used as the parking orbit. The PSO decision variables in this case are reduced to those identifying the manifold patch point (τ_h and τ_m) and η_{cut} is set to zero to simulate continuous thrust trajectories. The parking orbit (a_T) is also fixed. The value of GEO-energy, unreported in the original reference, is assumed to be 9.6 [43]. The comparison between the two cases is shown in Table 7. For each case calculated here, the best of ten PSO runs is reported – five for stable plus manifold, five for stable minus manifold, both of which approach Earth for the case of this large-amplitude halo orbit.

Table 7 Transfer to EML$_1$ halo orbit with A_z = 72000km

	Optimal cost (Equation 22)	$e_{terminate}$	Total TOF	Mass fraction consumed
Solution reported in [42]	0.1201	0.0019	≈116.077 days (26.73 TU)	6.0733%
Method used in [42]	0.1194	~0	116.767 days	6.1619%
QLEPSO	0.1286	0.0051	113.106 days	6.6692%

The optimal cost reported in the first row of Table 7 is taken from [42] and is included here in order to corroborate the current implementation of tangential thrust control law. Differences between the first two rows of Table 7 may arise due to inconsistencies in the value of GEO-energy or perturbation ϵ used for manifold generation. Another contributing factor could be the removal of the condition from [42] that τ_h take only certain discrete values. The QLEPSO solution also consumes more fuel due to the substantial change in inclination commanded in the problem setup, instead of the incidental change in inclination that can be achieved using tangential control.

Despite accounting for these factors, the results in the last two rows of Table 7 seem to indicate that tangential control law is more suitable for designing the LELT journey to the selected halo orbit. In order to demonstrate the real advantage of using Q-law over tangential thrust, this analysis is then repeated for the smaller halo orbit (EML$_1$ A_z≈8000km) defined in Table 5 and the results are presented in Table 8.

Table 8 Transfer to EML$_1$ halo orbit with A_z = 8000km

	Optimal cost (Equation 22)	$e_{terminate}$	Total TOF	Mass fraction consumed
Method used in [42]	0.4019	0.3128	60.4443 days	5.7770%
QLEPSO	0.1565	0.0068	93.6938 days	9.6227%

When designing transfers to the smaller halo orbit, the use of tangential control during the low-thrust arc is unable to circularize the orbit within the time required to achieve GEO-energy. The desired outcome of this trajectory design is to bring the eccentricity close to zero; the tangential control method is only able to achieve an eccentricity of 0.3128

using the objective function in Equation 22, whereas QLEPSO was able to bring it all the way to 0.0068, which is an almost circular orbit. This is in addition to accomplishing the high inclination change. Though the time of flight and fuel consumed are smaller in the case where tangential thrusting is used, it failed to produce feasible solutions where the essential condition regarding the parking orbit's eccentricity was satisfied. These results underscore the practicality of using QLEPSO when using more general settings. Furthermore, using the method developed in this paper allows for targeting of arbitrary parking orbits instead of only low-eccentricity, low-inclination orbits.

B. Use of Gradient-Based Methods

The accuracy of the LELT design method developed in the current work is quantified in this section by comparing our results with those obtained by using gradient-based methods. Apart from conveying the accuracy of solutions, this comparison will also demonstrate the advantage of QLEPSO in terms of computational efficiency. The first point of comparison is provided by previous studies that searched for locally minimum point solutions while minimizing a single objective function. This discussion is then concluded by showing comparable performance with a hybrid optimal control method that is capable of minimizing competing objectives.

Local Search: Minimum-Time Solutions

Mingotti et al. [7] conducted one of the earliest studies applying optimal control techniques to design (fixed I_{sp}) low-thrust transfers to halo orbits in the Earth-moon CR3BP via their manifolds. This early study ignored the inclination between GTO and the Earth-moon plane. Tangential thrusting was used for a majority of the thrust arc under the assumption that it allows for maximal increase in instantaneous energy. The simplifying assumptions used in [7] were removed by Martin et al. [12], where the control history along the entire thrust arc was optimized. The inclination of GTO was assumed to lie between 18.45° and 28.45°. A result from the work of Zhang et al. [44] is also used here, in which minimum-time low-thrust transfers were designed to *directly* transfer to a selected point on the halo orbit without traversing its stable manifold. Due to the modeling paradigm used in [44], the transfer reported here[‡] provides the approximate lower bound on the total time of flight from GTO to the EML_1 halo orbit of 8000 km out-of-plane amplitude. This means that the time-of-flight constraint applied to the problem must be greater than the ~56 days required for continuous thrust trajectories to reach the halo orbit. Throughout these comparisons, the applicable caveat is that the reported value of thrust acceleration used in the current paper is its *final* value (i.e., at delivery to the halo orbit) due to its inherent nature of backward propagation, while the referenced studies use the same value as their *initial* thrust acceleration. Table 9 catalogs the comparison of our results with these past analyses where a similar trajectory was designed from GTO to EML_1 halo orbit of A_z = 8000km. These QLEPSO runs are conducted by eliminating a_T as a design variable and instead fixing the initial parking orbit at GTO. The maximum allowable total time-of-flight is set

[‡]for the closest matching value of thrust acceleration

at 90 days.

The method developed in this paper generates solutions with mass delivery fractions within 3% of the optimal solutions found through deterministic gradient-based methods. The LELT trajectories in [7] and [12] consist of the same phases as in the QLEPSO method, where the spacecraft's orbit is raised using low-thrust engines until it is delivered to the stable manifold. The difference, however, is that while the referenced studies use continuous thrust to reach the manifold, our method allows coast arcs within the orbit raising phase. Due to the intrinsic nature of low-thrust trajectories, allowing coast arcs within a transfer reduces fuel consumption at the cost of longer flight times. In this case however, a spacecraft being delivered to the manifold is bound to spend time coasting on it anyway; this coast time is reallocated by the QLEPSO solution to the orbit raising phase with the purpose of reducing fuel consumption. This reassignment of coast locations is the root cause of low mass propellant consumption in the transfer designed using QLEPSO.

Table 9 Comparison with solutions from literature

	Orbit raising TOF (days)	Coast TOF on manifold (days)	Total TOF (days)	Mass fraction consumed
Mingotti et al. [7]	Unreported	Unreported	91.5	8.92%
Martin et al. [12]	47.1023	41.9463	89.0486	9.68%
Zhang et al. [44]	56.2458	-	56.2458	11.02%
QLEPSO	76.343	13.649	89.992	8.35%[§]

One of the primary goals of this paper is to ensure that the method developed here can achieve equivalent performance as traditional preliminary mission design methods with a much lower computational budget. A single QLEPSO run takes less than an hour to complete on a desktop computer with 4 cores running at 3.40GHz. On the other hand, the solutions generated by Martin et al. [12, 45] report a runtime on "order of days on a desktop computer". Though runtimes are not reported in the other works referenced in Table 9, it is expected to be on the order of tens of hours for every final solution generated [¶]. Also noteworthy is that using gradient-based methods usually involves generating and providing successive initial guesses through homotopy, like the process implemented in [12] and [44]. However, the comparison in Table 9 demonstrates that reasonable approximations to optimal trajectories can be obtained by using QLEPSO.

Local Search: Minimum-Fuel Solutions

In addition to applying gradient-based methods to finding minimum-*time* solutions for direct Earth-to-halo transfer, Zhang et al. [44] also continue the process to obtain minimum-*fuel* solutions for different thrust levels with specified TOFs. An attempt was made to design similar transfers using the method developed in this paper, by fixing $\tau_m = 0$ within the solution process. This implies that the transfer initiates delivery of the low-thrust spacecraft directly to the

[§] As a clarifying note, this value is higher than the result in Table 6 due to the high inclination of the parking orbit used here.

[¶] estimated based on computational time of 28h reported in [9] for a comparable problem

halo orbit, without leveraging its associated manifold. The selected EML_1 halo orbit (A_z = 8000 km) lies entirely within the lunar SOI, which means that QLEPSO may provide less effective solutions, though they will be fully feasible within the framework. These results are provided in Table 10, where the time-of-flight specified is obtained from [44] and serves as the constraint for our method. Specifically, this differs from the QLEPSO results in Table 9, where only transfers with 90 days flight time were calculated.

Table 10 Comparison with minimum-fuel solutions from Zhang et al. [44]

Thrust level	Total TOF	Mass fraction consumed in reference solutions [44]	Mass fraction consumed in QLEPSO solutions
0.6 N	140.2678 days	8.50%	8.13%
1 N	84.3688 days	8.69%	8.33%
2 N	37.8965 days	8.54%	8.69%
3 N	27.4773 days	9.12%	8.35%
5 N	16.8524 days	9.47%	8.95%

The propellant consumed in direct Earth-to-halo low-thrust trajectories designed using the QLEPSO method is lower than those found in [44]. This is due to the fact that the authors of the referenced work fixed the initial and final points of the transfer, i.e., the transfer commences at a GTO whose orientation (in terms of argument of periapse ω and longitude of ascending node Ω) is completely fixed, and ends at the point on the halo orbit where it achieves maximum separation from the Earth-moon plane. This is equivalent to fixing τ_h and τ_m in our formulation of the problem, as well as aiming for all orbital elements while designing the low-thrust orbit raising spiral. However, our Q-law implementation aims to definitively match only the semi-major axis, eccentricity and the inclination of the Earth parking orbit since the other elements can be targeted through the launch itself. Thus, the freedom of not targeting other orbital elements allows our method to produce better results. Regardless of matching the exact boundary conditions, the QLEPSO solution provides a close approximation of the transfer cost. As a point of note, the QLEPSO failed to converge when constraining the total TOF to the values reported in [44] for higher values of thrust. Acceptable solutions were found in these higher thrust cases when the time of flight constraint was relaxed.

Global Search Solutions

The hybrid optimal control framework developed by Shah et al. [46] provides a fully automated tool, now named DyLAN, for design of three-body transfer problems. It consists of a nested loop architecture to conduct global exploration of the search space associated with the problem. The outer loop uses a multi-objective genetic algorithm to pick the design variables that define the problem structure. This is complemented by the inner loop that solves the optimal control problem defined by the outer loop. The problem is defined to begin at the Earth parking orbit and thrust tangentially until a certain Jacobi energy is achieved. The spacecraft is then allowed one coast arc as well as another thrust arc to

reach the manifold patch point. The thrust arc beyond the main orbit-raising spiral is solved within the inner loop using the finite burn low thrust (FBLT) transcription. In this way, the boundary conditions of the optimal control problem supplied to the inner loop are decided by the outer loop. This hybrid optimal control framework is thus capable of generating the Pareto-front of time-of-flight vs. propellant mass consumed.

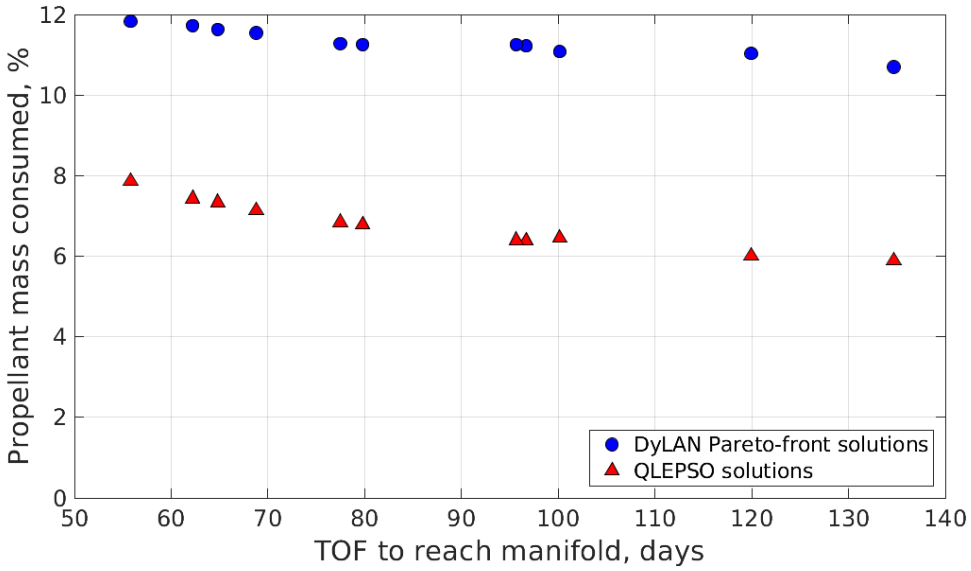

Fig. 4 Comparison with DyLAN solutions from [30]

The final comparison of the QLEPSO method is conducted against the results obtained by the DyLAN framework in [30]. The cost of these transfers, designed between a GTO and an EML_1 halo orbit of A_z = 5000 km, is charted in Fig. 4. These reference trajectories correspond to a thrust acceleration of 1×10^{-3} m/s^2. As before, due to the difference in direction of trajectory propagation, this thrust acceleration is the *final* value in the case of QLEPSO, and the *initial* value for DyLAN. The Pareto-front of DyLAN solutions in Fig. 4 was produced by using multi-objective optimization techniques. The QLEPSO data points, however, were obtained one-by-one by setting the TOF constraint to match the referenced results. The important distinction from the previous case comparisons is that only the time to reach the stable manifold is counted for flight time calculation. This is done in order to match the settings of the reported results in [30] and is achieved by excluding the $|\tau_m|$ term from the TOF constraint in Equation 19.

As explained earlier, the DyLAN solutions consist of a continuous tangential thrust arc starting at the parking orbit, followed by a coast arc and another thrust arc as decided by the outer loop solver. At the end of these phases, the spacecraft is delivered to the manifold. Thus the FBLT transcription is used only to optimize the second thrust arc. In Fig. 4, the same trend of reallocation of coast arcs by QLEPSO is observed – the coast arc is removed from the pre-FBLT section and reassigned to the orbit-raising phase. Due to this, all QLEPSO-designed transfers consume less fuel than the DyLAN solutions.

VI. Conclusions

This paper describes a design method for quantifying low-energy, low-thrust transfers in a three-body system in a computationally efficient manner. It uses the previously proposed Q-law, a feedback control law based on Lyapunov control theory, to design the low-thrust trajectory, combining it with low-energy dynamical systems theory. This low-energy low-thrust (LELT) trajectory design problem is parametrized by the initial parking orbit, Q-law weights and effectivity cutoff, and the manifold patch point. These decision variables are optimized using a particle swarm algorithm. A simple and effective strategy, comprising of marking infeasible solutions with fictitious high fitness values, is implemented here to deal with the time-of-flight constraint. The complete technique is demonstrated on the design of a transfer that starts at an Earth parking orbit and uses low-thrust propulsion to transport the spacecraft to the stable manifold of an Earth-moon L_1 halo orbit within a specified flight time. The optimal solutions thus obtained show that the insertion on the invariant manifold occurs at the closest allowed points to the halo orbit in order to spread the coasting time all along the low-thrust section of the trajectory. The parking orbit, constrained by the Δv to transfer from LEO to GTO, was also chosen to have the highest achievable apogee, with minimal inclination change.

Close agreement between the results obtained here and the optimal solutions obtained through gradient-based deterministic methods serves the purpose of validating and assessing the applicability of the developed preliminary Q-law LELT trajectory design with PSO (or simply QLEPSO) method. In addition to its accuracy, QLEPSO also provides significant savings in computational effort due to the use of the non-iterative Q-law for low-thrust arc design. By itself, the estimates provided by this method for percentage mass propellant consumed are suitable for large-scale trade space studies or logistics planning. This method is also well suited for use in the preparatory stages for gradient-based solving techniques (i.e., for seeding initial guesses); the use of QLEPSO for achieving higher-fidelity solutions in this manner is an open avenue of future work.

Appendix: Physical Constants

Table 11 Values of physical constants used in current study

Parameter	Value
Mass parameter μ	0.012150585609624
Standard gravity g	9.809 m/sec^2
Distance unit (DU) in rotating frame (also $a_{\leftmoon}$)	384400 km
Time unit (TU) in rotating frame	375197.691775973 sec
Lunar mean motion $n_{\leftmoon}$	2.64907088×10^{-6} rad/sec

References

[1] Howell, K., Barden, B., and Lo, M., "Application of Dynamical Systems Theory to Trajectory Design for a Libration Point Mission," *The Journal of the Astronautical Sciences*, Vol. 45, No. 2, 1997, pp. 161–178.

[2] Anderson, R. L., and Lo, M. W., "Role of Invariant Manifolds in Low-Thrust Trajectory Design," *Journal of Guidance, Control, and Dynamics*, Vol. 32, No. 6, 2009, pp. 1921–1930. doi:10.2514/1.37516.

[3] Farquhar, R. W., "The Utilization of Halo Orbits in Advanced Lunar Operations," *NASA Technical Note D-6365*, 1971.

[4] Parker, J. S., and Born, G. H., "Modeling a Low-Energy Ballistic Lunar Transfer Using Dynamical Systems Theory," *Journal of Spacecraft and Rockets*, Vol. 45, 2008, pp. 1269–1281. doi:10.2514/1.35262.

[5] Senent, J., Ocampo, C., and Capella, A., "Low-Thrust Variable-Specific-Impulse Transfers and Guidance to Unstable Periodic Orbits," *Journal of Guidance, Control, and Dynamics*, Vol. 28, No. 2, 2005, pp. 280–290. doi:10.2514/1.6398.

[6] Ozimek, M., and Howell, K., "Low-Thrust Transfers in the Earth-Moon System, including Applications to Libration Point Orbits," *Journal of Guidance, Control, and Dynamics*, Vol. 33, No. 2, 2010, pp. 533–549. doi:10.2514/1.43179.

[7] Mingotti, G., Topputo, F., and Bernelli-Zazzera, F., "Combined Optimal Low-Thrust and Stable-Manifold Trajectories to the Earth-Moon Halo Orbits," *AIP Conference Proceedings*, Vol. 886, 2007, pp. 100–112. doi:10.1063/1.2710047.

[8] Mingotti, G., Topputo, F., and Bernelli-Zazzera, F., "Low-Energy, Low-Thrust Transfers to the Moon," *Celestial Mechanics and Dynamical Astronomy*, Vol. 105, No. 1-3, 2009, p. 61. doi:10.1007/s10569-009-9220-7.

[9] Mingotti, G., Topputo, F., and Bernelli-Zazzera, F., "Optimal Low-Thrust Invariant Manifold Trajectories via Attainable Sets," *Journal of Guidance, Control, and Dynamics*, Vol. 34, No. 6, 2011, p. 1644. doi:10.2514/1.52493.

[10] Mingotti, G., Topputo, F., and Bernelli-Zazzera, F., "Transfers to Distant Periodic Orbits around the Moon via their Invariant Manifolds," *Acta Astronautica*, Vol. 79, 2012, pp. 20–32. doi:10.1016/j.actaastro.2012.04.022.

[11] Mingotti, G., Sánchez, J., and McInnes, C., "Combined Low-Thrust Propulsion and Invariant Manifold Trajectories to Capture NEOs in the Sun–Earth Circular Restricted Three-Body Problem," *Celestial Mechanics and Dynamical Astronomy*, Vol. 120, No. 3, 2014, pp. 309–336. doi:10.1007/s10569-014-9589-9.

[12] Martin, C., and Conway, B. A., "Optimal Low-Thrust Trajectories Using Stable Manifolds," *Spacecraft Trajectory Optimization*, edited by B. A. Conway, Cambridge University Press, 2010, Chap. 9. doi:10.1017/CBO9780511778025.010.

[13] Mingotti, G., and Gurfil, P., "Mixed Low-Thrust Invariant-Manifold Transfers to Distant Prograde Orbits around Mars," *Journal of Guidance, Control, and Dynamics*, Vol. 33, No. 6, 2010, pp. 1753–1764. doi:10.2514/1.49810.

[14] Mingotti, G., Topputo, F., and Bernelli-Zazzera, F., "Earth–Mars Transfers with Ballistic Escape and Low-Thrust Capture," *Celestial Mechanics and Dynamical Astronomy*, Vol. 110, No. 2, 2011, pp. 169–188. doi:10.1007/s10569-011-9343-5.

[15] Petropoulos, A. E., and Longuski, J. M., "Shape-Based Algorithm for the Automated Design of Low-Thrust, Gravity Assist Trajectories," *Journal of Spacecraft and Rockets*, Vol. 41, No. 5, 2004, pp. 787–796. doi:10.2514/1.13095.

[16] Izzo, D., "Lambert's Problem for Exponential Sinusoids," *Journal of Guidance, Control, and Dynamics*, Vol. 29, No. 5, 2006, pp. 1242–1245. doi:10.2514/1.21796.

[17] Wall, B. J., and Conway, B. A., "Shape-Based Approach to Low-Thrust Rendezvous Trajectory Design," *Journal of Guidance, Control, and Dynamics*, Vol. 32, No. 1, 2009, pp. 95–101. doi:10.2514/1.36848.

[18] Vellutini, E., and Avanzini, G., "Shape-Based Design of Low-Thrust Trajectories to Cislunar Lagrangian Point," *Journal of Guidance, Control, and Dynamics*, Vol. 37, No. 4, 2014, pp. 1329–1335. doi:10.2514/1.G000165.

[19] Chang, D. E., Chichka, D. F., and Marsden, J. E., "Lyapunov-Based Transfer between Elliptic Keplerian Orbits," *Discrete and Continuous Dynamical Systems Series B*, Vol. 2, No. 1, 2002, pp. 57–68. doi:10.3934/dcdsb.2002.2.57.

[20] Petropoulos, A., "Low-Thrust Orbit Transfers using Candidate Lyapunov Functions with a Mechanism for Coasting," *AIAA/AAS Astrodynamics Specialist Conference*, August 2004. doi:10.2514/6.2004-5089.

[21] Kluever, C. A., "Simple Guidance Scheme for Low-Thrust Orbit Transfers," *Journal of Guidance, Control, and Dynamics*, Vol. 21, No. 6, 1998, pp. 1015–1017. doi:10.2514/2.4344.

[22] Ruggiero, A., Pergola, P., Marcuccio, S., and Andrenucci, M., "Low-Thrust Maneuvers for the Efficient Correction of Orbital Elements," *32nd International Electric Propulsion Conference*, Paper IEPC-2011-102, September 2011, pp. 11–15.

[23] Petropoulos, A., and Lee, S., "Optimisation of Low-Thrust Orbit Transfers Using the Q-Law for the Initial Guess," *AAS/AIAA Astrodynamics Specialist Conference*, AAS Paper 05–392, August 2005.

[24] Lee, S., von Ailmen, P., Fink, W., Petropoulos, A., and Terrile, R. J., "Design and Optimization of Low-Thrust Orbit Transfers," *IEEE Aerospace Conference*, March 2005. doi:10.1109/AERO.2005.1559377.

[25] Jagannatha, B. B., and Ho, K., "Optimization of In-Space Supply Chain Design Using High-Thrust and Low-Thrust Propulsion Technologies," *Journal of Spacecraft and Rockets*, Vol. 55, No. 3, 2018, pp. 648–659. doi:10.2514/1.A34042.

[26] Richardson, D. L., "Analytic Construction of Periodic Orbits about the Collinear Points," *Celestial Mechanics and Dynamical Astronomy*, Vol. 22, No. 3, 1980, pp. 241–253. doi:10.1007/BF01229511.

[27] Petropoulos, A., "Refinements to the Q-law for Low-Thrust Orbit Transfers," *AAS/AIAA Space Flight Mechanics Conference*, AAS Paper 05-162, January 2005.

[28] Whiffen, G., "Mystic: Implementation of the Static Dynamic Optimal Control Algorithm for High-Fidelity, Low-Thrust Trajectory Design," *AIAA/AAS Astrodynamics Specialists Conference*, August 2006. doi:10.2514/6.2006-6741.

[29] Petropoulos, A. E., Tarzi, Z. B., Lantoine, G., Dargent, T., and Epenoy, R., "Techniques for Designing Many-Revolution Electric-Propulsion Trajectories," *AAS/AIAA Space Flight Mechanics Meeting*, AAS Paper 14-373, January 2014.

[30] Jagannatha, B. B., Shah, V., Beeson, R., and Ho, K., "Exploration of Low-Thrust Trajectories to Earth-Moon Halo Orbits," *AIAA/AAS Astrodynamics Specialist Conference*, AIAA Paper 17-757, August 2017.

[31] Vesterstrom, J., and Thomsen, R., "A Comparative Study of Differential Evolution, Particle Swarm Optimization, and Evolutionary Algorithms on Numerical Benchmark Problems," *Congress on Evolutionary Computation*, Vol. 2, IEEE, 2004, pp. 1980–1987. doi:10.1109/CEC.2004.1331139.

[32] Kennedy, J., and Eberhart, R., "Particle Swarm Optimization," *IEEE International Conference on Neural Networks*, Vol. 4, 1995, pp. 1941–1948. doi:10.1109/ICNN.1995.488968.

[33] Parsopoulos, K. E., Vrahatis, M. N., et al., "Particle Swarm Optimization Method for Constrained Optimization Problems," *Intelligent Technologies–Theory and Application*, edited by V. Kvasnicka, J. Pospíchal, and P. Sincák, IOS Press, 2002, pp. 214–220.

[34] Perez, R. l., and Behdinan, K., "Particle Swarm Approach for Structural Design Optimization," *Computers & Structures*, Vol. 85, No. 19-20, 2007, pp. 1579–1588. doi:10.1016/j.compstruc.2006.10.013.

[35] Pontani, M., and Conway, B. A., "Particle Swarm Optimization Applied to Space Trajectories," *Journal of Guidance, Control, and Dynamics*, Vol. 33, No. 5, 2010, pp. 1429–1441. doi:10.2514/1.48475.

[36] "Particle Swarm Optimization Algorithm," MATLAB R2016a. URL `https://www.mathworks.com/help/gads/particle-swarm-optimization-algorithm.html`, [retrieved 15 May 2018].

[37] Dormand, J. R., and Prince, P. J., "Higher Order Embedded Runge—Kutta Formulae," *Journal of Computational and Applied Mathematics*, Vol. 7, No. 1, 1981, pp. 67–75. doi:10.1016/0771-050X(81)90010-3.

[38] "Moon Fact Sheet," NASA. URL https://nssdc.gsfc.nasa.gov/planetary/factsheet/moonfact.html, [retrieved 30 Jan 2018].

[39] Parker, J. S., "Low-Energy Ballistic Lunar Transfers," Ph.D. thesis, University of Colorado at Boulder, 2007.

[40] Kluever, C. A., "Designing Transfers to Geostationary Orbit Using Combined Chemical–Electric Propulsion," *Journal of Spacecraft and Rockets*, Vol. 52, No. 4, 2015, pp. 1144–1151. doi:10.2514/1.A33259.

[41] Arora, N., and Strange, N., "A Low Energy, Low Thrust Unified Solver for Rapid Mission Design," *AAS/AIAA Space Flight Mechanics Meeting*, AAS Paper 13-255, February 2013.

[42] Abraham, A. J., Spencer, D. B., and Hart, T. J., "Early Mission Design of Transfers to Halo Orbits via Particle Swarm Optimization," *The Journal of the Astronautical Sciences*, Vol. 63, No. 2, 2016, pp. 81–102. doi:10.1007/s40295-016-0084-2.

[43] Parker, J. S., and Anderson, R. L., "Low-Energy Lunar Trajectory Design," JPL DESCANSO Series, John Wiley & Sons, 2014, Chap. 2. doi:10.1002/9781118855065.

[44] Zhang, C., Topputo, F., Bernelli-Zazzera, F., and Zhao, Y.-S., "Low-Thrust Minimum-Fuel Optimization in the Circular Restricted Three-Body Problem," *Journal of Guidance, Control, and Dynamics*, Vol. 38, No. 8, 2015, pp. 1501–1510. doi:10.2514/1.G001080.

[45] Martin, C., "A New Numerical Optimization Method Based on Taylor Series for Challenging Trajectory Optimization Problems," Ph.D. thesis, University of Illinois at Urbana-Champaign, 2011.

[46] Shah, V., Beeson, R., and Coverstone, V., "Automated Global Optimization of Multi-Phase Trajectories in the Three-Body Problem using a Variable Chromosome Transcription," *AAS/AIAA Space Flight Mechanics Conference*, AAS Paper 17-445, February 2017.